preprint of article in J. Magn. Reson. 173, 229-235 (2005)

Pattern Pulses: Design of arbitrary excitation profiles as a function of pulse amplitude and offset

Kyryl Kobzar [1], Burkhard Luy [1], Navin Khaneja [2], Steffen J. Glaser [1]

[1]Department of Chemistry, Technische Universität München,
Lichtenbergstr. 4, 85747 Garching, Germany

[2]Division of Applied Sciences, Harvard University, Cambridge, MA 02138, USA

Abstract

A novel class of pulses is presented which can be regarded as a generalization of both frequency-selective pulses and B_1-selective pulses. The excitation profile of these pulses forms a pre-defined pattern in two dimensions, which are spanned by pulse offset and rf amplitude. The presented pulses were designed numerically based on principles of optimal control theory. For simple test patterns, we demonstrate the flexibility of this approach by simulations and experiments. This previously unknown flexibility may trigger novel applications in NMR spectroscopy and imaging. As a first practical application, we demonstrate a direct approach for calibrating rf pulses.

1 Introduction

Radio-frequency pulses with defined excitation or inversion profiles have a long history in NMR (1-6). Pulses which are selective, band-selective and broadband with respect to offset and/or rf amplitude have found numerous applications in NMR spectroscopy and imaging. A particularly powerful approach for the design of such pulses is based on principles of optimal control theory (7-10), which make it possible to optimize a large number of pulse-sequence parameters very efficiently. As conventional approaches were typically limited to a few dozens of pulse parameters, a typical strategy was to restrict the optimization to certain pulse families, such as composite pulses with a limited number of flip and phase angles (1, 4), Gaussian pulse cascades (11), spline functions (12) or Fourier expansions (13, 14). In contrast, the number of pulse parameters that can be optimized by optimal control based algorithms can be several orders of magnitude larger compared to conventional approaches. In NMR, this approach has been used so far to design band-selective pulses (9, 15-17), robust broadband excitation and inversion pulses (18-21) and to explore the physical limits of pulse performance (20). Here, we demonstrate the design of pulses which create arbitrary patterns as a function of offset and rf amplitude.

2 Theory

We consider an uncoupled spin 1/2 with offset frequency ν_0 which is subject to radio frequency (rf) irradiation of duration τ. The rf irradiation is characterized by its (nominal) maximum rf amplitude $\nu_1 = -\gamma B_1^{max}/(2\pi)$ and by the two real functions $\phi(t)$ and $s(t)$, where $\phi(t)$ is the phase of the rf field and $s(t)$ represents the shape function of the rf amplitude modulation, which is positive and scaled such that the maximum value of $s(t)$ is 1.

Here, we restrict the following discussion to excitation pulses that create x magnetization if applied to initial z magnetization. However, the results can be immediately generalized

to other pulses, such as saturation or inversion pulses. (In fact, the design of selective inversion pulses is generally considered to be an easier problem than the design of selective excitation pulses (5, 22).)

For conventional pulses, the desired excitation profile as a function of offset (ν_0) and rf amplitude (ν_1) typically has the form of a rectangle. The width $\Delta\nu_0$ of this rectangular profile corresponds to the bandwidth of frequency offsets to be covered, whereas the height $\Delta\nu_1$ of the rectangle specifies the range of rf amplitudes ν_1 for which the pulse is expected to be functional. For example, for a broadband excitation pulse which is also robust with respect to rf amplitude variations due to pulse miscalibration or due to rf inhomogeneity, both $\Delta\nu_0$ and $\Delta\nu_1$ should be large, see e.g. (18-21, 23-27). In contrast, for offset-selective or rf amplitude-selective pulses, $\Delta\nu_0$ or $\Delta\nu_1$ should be small, respectively (4, 5, 22, 28-36). However, as shown below, it is possible to create much more sophisticated patterns of excitation as a function of ν_0 and ν_1.

In Fig. 1 A-D, a series of simple test patterns is shown. In these examples, the test patterns were specified as the desired orientation of the target magnetization vector M_t after the pulse (white: $M_t = (1, 0, 0)$, black: M_t=(0, 0, 1)) on a grid of N_0 equally spaced offsets ν_0 between -5 kHz and $+5$ kHz (but $\pm$ 10 kHz in Fig. 1 B) and N_1 equally spaced rf amplitudes ν_1 between 6 kHz and 14 kHz. Here, the $N_0 \times N_1$ grid of offsets and rf amplitudes, for which the desired M_x component was specified, was chosen to be 40×16 (Fig. 1A), 105×10 (Fig. 1B), and 40×10 (Fig. 1C, D).

Fig. 1A represents an excitation profile that is band-selective with respect to rf amplitude (9 kHz $\leq \nu_1 \leq$ 11 kHz) and broadband with respect to offset (-5 kHz $\leq \nu_0 \leq$ 5 kHz). Conversely, Fig. 1B represents a profile that is narrowband with respect to offset (-1 kHz $\leq \nu_0 \leq$ 1 kHz) and broadband with respect to rf amplitude (6 kHz $\leq \nu_1 \leq$ 14 kHz). Figures 1 C and D represent more general excitation patterns that cannot be specified by a rectangular excitation region with band widths $\Delta\nu_0$ and $\Delta\nu_1$. The pattern in Fig. 1C corresponds to a pulse that excites spins at different offsets, depending on the rf

amplitude. In particular, here the desired excitation freqency ν_0 was proportional to ν_1. Conversely, the pattern in Fig. 1D excites x magnetization for all combinations of ν_0 and ν_1 in the given range, except for offsets that are proportional to the rf amplitude.

For these target patterns, we optimized rf pulses using the general optimal control based gradient ascent strategy with the cost (21)

$$\Phi = \sum_{\nu_0} \sum_{\nu_1} \|\vec{M}_t(\nu_0, \nu_1) - \vec{M}_f(\nu_0, \nu_1)\|^2,$$

where M_f is the final magnetization vector after a given pulse, M_t is the target vector, as specified in Fig. 1 A-D. In general, larger pulse durations result in larger flexibility of the achievable excitation pattern. Here, we chose pulse durations of 2, 3, 5, and 5 ms. Each pulse was digitized in steps of 0.5 μs and the x and y amplitudes of all subpulses were optimized (18, 19). For example, for a pulse duration of 5 ms, this corresponds to 20000 optimization parameters. The amplitude and phase functions $s(t)$ and $\phi(t)$ of the resulting pulses are shown in Figs. 2 A-D. The performance of the optimized pulses was first analyzed by simulating the excitation profiles numerically for the same range of offsets and rf amplitudes as in Figs. 1 A-D (but on a finer grid of 100×21 combinations of ν_0 and ν_1). In all cases, a reasonable match is found between desired and simulated excitation profiles.

The examples shown in Fig. 1 suggest that the power and flexibility of the optimum control gradient ascent algorithm will allow to create arbitrary excitation patterns, provided the specified pulse duration is suffiently long. As a non-trivial test case, we specified the more complex pattern shown in Fig. 3. Here, the target pattern was defined on a grid of $N_0 = 120$ equally spaced offsets ν_0 between ± 10 kHz and $N_1 = 20$ equally spaced rf amplitudes between 6 kHz and 14 kHz. A pulse with a duration of 5 ms was optimized (data not shown), which created the simulated excitation pattern shown in Fig. 3 B.

3 Experimental

The new pattern pulses were tested experimentally using a sample of 99.96% D_2O doped with $CuSO_4$ to a final T_1 relaxation time of $\sim$ 500 ms. This solution was placed in a 5 mm Shigemi limited volume tube with a very restricted active volume of only 20 μl in order to reduce the B_1 field inhomogeneity in the sample. The experiments were performed on a Bruker Avance spectrometer equipped with modern SGU units for RF control and linearized amplifiers.

We used two different approaches to acquire the experimental ν_0-ν_1 pattern of a given pulse. In the first approach, a spectrum of the sample is acquired for each combination of ν_0 and ν_1. The resulting peak amplitude as a function of offset and rf amplitude respresents the experimental excitation pattern. For example, for N_0=41 offset values and N_1=20 different rf amplitude settings, this requires the acquisition of N_0N_1= 820 scans. Hence, with a typical delay of 1 s between scans, the acquisition of a detailed two-dimensional excitation pattern requires about 14 minutes.

Alternatively, for each rf amplitude ν_1, the response of the spins can be simultaneously acquired for a desired offset range in a single shot by performing the experiments in the presence of a B_0 field gradient (37, 38). As we were interested only in the x component of the final magnetization vectors, we used the following variant of the single shot experiment, which is insensitive to imperfect gradient switching (c.f. Fig. 4). The experiment exploits the excellent broadband excitation characteristics of BEBOP pulses (18, 19), which have been calibrated and tested on our spectrometer before. Here, we used a BEBOP pulse with a maximum rf amplitude of ν_1=17.5 kHz and a duration of 125 μs (21), which transforms z magnetization to x magnetization over a bandwidth of 40 kHz. (For actual calibration experiments, a more robust pulse, such as the 500 μs BEBOP pulse should be used, which is insensitive to ν_1 variations of about $\pm$ 2 dB (19)). Immediately after the shaped pulse of interest is applied to the sample, the resulting x magnetization is flipped to the z axis by

a time-reversed BEBOP pulse. Any remaining transverse magnetization is defocused by the gradient during a delay $\delta = 1.2$ ms and finally the stored z magnetization is brought back to the x axis by the BEBOP pulse and is detected. Fourier transformation of the FID yields the excitation profile of the shaped pulse of interest. The single shot approach for each ν_1 setting significantly reduces the time required to measure the experimental excitation pattern as a function of ν_0 and ν_1, e.g. in the example given above, the time is reduced from 14 minutes to only 20 seconds. A disadvantage of the single-shot approach is that distorted patterns can result if B_0 gradient and B_1 inhomogeneity are spatially correlated. Conversely, this effect may be useful to measure such correlations.

Figs. 1 A″-D″ and 2 C show experimental excitation patterns acquired using the first approach for N_0=41 different offsets ν_1 and N_1=17 different rf amplitudes (except for Fig. 1 A″, where N_1=20). In all cases, an excellent match is found between simulated and experimental excitation patterns.

4 Calibration pulses

The simple patterns created in this exploratory study are reminiscent of early test patterns used to calibrate TV sets. For example, in 1934, the BBC used a simple test card which showed a circle over a horizontal line (39). In the following decades, more sophisticated test patterns were designed and are still being used by engineers to calibrate monitors. Similarly, specifically designed pattern pulses could also become a useful tool for setting up experiments and testing spectrometer hardware.

As an illustrative example, consider the calibration of rf amplitudes. The simple pattern shown in Fig. 1 C directly translates rf amplitude into excitation frequency and hence, the rf amplitude ν_1 can be directly infered from the excitation frequency in a single shot experiment. The flexibility of pattern pulses makes it possible to design more sophisti-

cated calibration pulses which provide internal "tick marks" to directly quantify a given rf misadjustment. To illustrate this approach, we designed the test pattern shown in Fig. 5 A for the calibration of a rf pulse with an amplitude ν_1 of 10 kHz. The desired excitation pattern consists of five separate frequency bands at the offsets 0 kHz, ± 1.5 kHz, and ± 3.5 kHz, which were designed to have different bandwidths in order to be easily distinguishable. For the desired rf amplitude of 10 kHz, the central band at an offset of 0 kHz is not excited, whereas the bands at -1.5 kHz and -3.5 kHz are negative (corresponding to $-x$ magnetization) and the bands at +1.5 kHz and +3.5 kHz are positive (corresponding to $+x$ magnetization). If the actual rf amplitude is only 6 kHz, all five bands in the excitation profile are positive, whereas for an rf amplitude of 14 kHz, all five bands are negative. For any intermediate rf amplitude, the resulting excitation profile as a function of ν_0 allows to determine the actual misadjustment of the rf amplitude. A corresponding pulse with a duration of 6 ms was optimized to create this pattern and the simulated excitation profile is shown in Fig. 5 B. Fig. 5 C shows seven experimental single shot spectra for rf amplitudes between 6.3 and 14.1 kHz, corresponding to rf amplitude missettings between +4 and -3 dB. Each of these spectra would allow to determine the necessary attenuator correction to achieve the desired pulse amplitude. In practice, several such calibration pulses with different grid resolution could be used for rough and subsequent fine adjustment of the rf power level.

5 Discussion

We demonstrated the ability to design complex excitation patterns as a function of offset and rf amplitude, using efficient optimization algorithms based on ideas from optimal control theory. Clearly, the achievable resolution in ν_0 and ν_1 of a desired excitation pattern depends on the pulse duration, the pulse digitization and the number of optimization parameters. A detailed study of these relations is beyond the scope of this paper but will

be an interesting subject for future investigations. In the present study, we used pulse durations between 2 and 6 ms and up to 24000 optimization parameters, which resulted in practical pulses. This study as well as previous studies (18, 19, 21) clearly show that state of the art spectrometers can inplement complicated pulses defined in a shape file with the same ease as much simpler pulses. We expect that the ability to create virtually arbitrary excitation patterns as a function of ν_0 and ν_1 will find numerous applications in NMR spectroscopy and imaging. For example, the flexibility of pattern pulses makes it possible to excite a predefined region of interest in localized NMR experiments in the presence of both B_0 and B_1 gradients. As a simple example, we demonstrated the use of a specifically designed test pattern for B_1 calibration. The presented pattern pulses are point-to-point transformations that rotate a given initial magnetization vector to a desired final vector, however the methodology is also applicable to the development of potentially useful general rotation pulses.

Pulses described in this communication can be downloaded in Bruker format from http://www.org.chemie.tu-muenchen.de/people/bulu/.

Acknowledgments

B. L. thanks the Deutsche Forschungsgemeinschaft (Emmy Noether fellowship LU 835/1-2) for support. N. K. would like to thank Darpa Grant F496020-0101-00556. S. J. G. acknowledges support from the Deutsche Forschungsgemeinschaft (Grant Gl 203/4-2).

References

[1] M. H. Levitt, Composite pulses, *Prog. NMR Spectrosc.* **18**, 61-122 (1986).

[2] W. S. Warren and M.S. Silver, The Art of Pulse Crafting: Applications to Magnetic Resonance and Laser Spectroscopy, *Adv. Magn. Reson.* **12**, 247-384 (1988).

[3] D. Abramovich, S. Vega, Derivation of broadband and narrowband excitation pulses using the Floquet Formalism, *J. Magn. Reson. A* **105**, 30-48 (1993).

[4] M. H. Levitt, Composite pulses, in Encyclopedia of Nuclear Magnetic Resonance, 1396-1411, (Eds.-in-Chief D.M.Grant and R.K.Harris), John Wiley & Sons, Chichester-NewYork-Brisbane-Singapore, 1996.

[5] L. Emsley, Selective pulses, in Encyclopedia of Nuclear Magnetic Resonance, 4228-4236, (Eds.-in-Chief D.M.Grant and R.K.Harris), John Wiley & Sons, Chichester-NewYork-Brisbane-Singapore, 1996.

[6] R. Freeman, Shaped radiofrequency pulses in high resolution NMR, *Prog. NMR Spectrosc.* **32**, 59-106 (1998).

[7] A. Bryson, Jr., Y.-C. Ho, Applied optimal control, Hemisphere, Washington, D.C., 1975.

[8] D. J. Tannor, S. A. Rice, Control of selectivity of chemical reaction via control of wave packet evolution, *J. Chem. Phys.* **83**, 5013-5018 (1985).

[9] S. Conolly, D. Nishimura, A Macovski, Optimal control solutions to the magnetic resonance selective excitation problem, *IEEE Trans. Med. Imaging* **MI-5**, 106-115 (1986).

[10] N. Khaneja, T. Reiss, C. Kehlet, T. Schulte-Herbrüggen, S. J. Glaser, Design of NMR Pulse Sequences by Gradient Ascent Algorithms, *J. Magn. Reson.*, submitted (2004).

[11] L. Emsley, G. Bodenhausen, Gaussian pulse cascades: new analytical functions for rectangular selective inversion and in-phase excitation in NMR, *Chem. Phys. Lett.* **165**, 469-476 (1990).

[12] B. Ewing, S. J. Glaser and G. P. Drobny, Development and optimization of shaped NMR pulses for the study of coupled spin systems, *Chem. Phys.* **147**, 121-129 (1990).

[13] D. B. Zax, G. Goelman, S. Vega, Amplitude-modulated composite pulses, *J. Magn. Reson.* **80**, 375-382 (1988).

[14] H. Geen, S. Wimperis, R. Freeman, Band-selective pulses without phase distortions. A simulated annealing approach, *J. Magn. Reson.* **85**, 620-627 (1989).

[15] J. Mao, T.H. Mareci, K.N. Scott, and E.R. Andrew, Selective inversion radiofrequency pulses by optimal control, *J. Magn. Reson.* **70**, 310-318 (1986).

[16] V. Smith, J. Kurhanewicz, T. James, Solvent-suppression pulses. I. Design using optimal control theory, *J. Magn. Reson.* **95**, 41-60 (1991).

[17] D. Rosenfeld and Y. Zur, Design of adiabatic selective pulses using optimal control theory, *Magn. Reson. Med.* **36**, 401-409 (1996).

[18] T. E. Skinner, T. O. Reiss, B. Luy, N. Khaneja, and S. J. Glaser, Application of optimal control theory to the design of broadband excitation pulses for high resolution NMR, *J. Magn. Reson.* **163**, 8-15 (2003).

[19] T. E. Skinner, T. O. Reiss, B. Luy, N. Khaneja, and S. J. Glaser, Reducing the duration of broadband excitation pulses using optimal control with limited RF amplitude, *J. Magn. Reson.* **167**, 68-74 (2004)

[20] K. Kobzar, T. E. Skinner, N. Khaneja, S. J. Glaser, B. Luy, Exploring the limits of broadband excitation and inversion pulses, *J. Magn. Reson.* **170**, 236-243 (2004).

[21] T. E. Skinner, T. O. Reiss, B. Luy, N. Khaneja, S. J. Glaser, Tailoring the optimal control cost function to a desired output: Application to minimizing phase errors in short broadband excitation pulses, *J. Magn. Reson.*, in press (2004).

[22] P. Charmont, D. Sakellariou, L. Emsley, Sample restriction using radiofrequency field selective pulses in high-resolution solid-state NMR, *J. Magn. Reson.* **154**, 136-141 (2002).

[23] M. Garwood, Y. Ke, Symmetric pulses to induce arbitrary flip angles with compensation for rf inhomogeneity and resonance offsets, *J. Magn. Reson.* **94**, 511-525 (1991).

[24] V. L. Ermakov, G. Bodenhausen, Broadband excitation in magnetic resonance by self-refocusing doubly frequency-modulated pulses, *Chem. Phys. Lett.* **204**, 375-380 (1993).

[25] $\overline{\text{E}}$ Kupče, R. Freeman, Wideband excitation with polychromatic pulses, *J. Magn. Reson. A* **108**, 268-273 (1994).

[26] M. A. Smith, H. Hu, A. J. Shaka, Improved broadband inversion performance for NMR in liquids, *J. Magn. Reson.* **151**, 269-283 (2001).

[27] K. E. Cano, M. A. Smith, A. J. Shaka, Adjustable, broadband, selective excitation with uniform phase, *J. Magn. Reson.* **155**, 131-139 (2002).

[28] D. I. Hoult, The solution of the Bloch equations in the presence of a varying B_1 field − An approach to selective pulse analysis, *J. Magn. Reson.* **35**, 69-86 (1979).

[29] M. R. Bendall, R. E. Gordon, Depth and refocusing pulses designed for multipulse NMR with surface coils *J. Magn. Reson.* **53**, 365-385 (1983).

[30] R. Tycko, A. Pines, Spatial Localization of NMR signals by narrowband inversion, *J. Magn. Reson.* **60**, 156-160 (1984).

[31] A. J. Shaka, R. Freeman, A composite 180° pulse for spatial localization, *J. Magn. Reson.* **63**, 596-600 (1985).

[32] A. J. Shaka, R. Freeman, "Prepulses" for spatial localization, *J. Magn. Reson.* **64**, 145-150 (1985).

[33] D. G. Cory, A DANTE-based method for radiofrequency-field selection, *J. Magn. Reson. A* **103**, 23-26 (1993).

[34] K. Scheffler, Design of B_1-insensitive and B_1-selective pulses by means of stochastic optimization, *J. Magn. Reson. B* **109**, 175-183 (1995).

[35] S. Wimperis, Broadband, narrowband, and passband composite pulses for use in advanced NMR experiments, *J. Magn. Reson. A* **109**, 221-231 (1994).

[36] R. Kemp-Harper, P. Styles, S. Wimperis, B_1-selective pulses, *J. Magn. Reson. A* **123**, 230-236 (1996).

[37] V. Belle, G. Cros, H. Lahrech, P. devoulon, M. Decorps, A rapid phase-sensitive method for measurement of the excitation profile of a shaped pulse, *J. Magn. Reson. A* **112**, 122-125 (1995).

[38] S. Berger, NMR Techniques Employing Selective Radiofrequency Pulses in Combination with Pulsed Field Gradients, *Progr. NMR Spectr.* **30**, 137-156 (1997).

[39] http://history.acusd.edu/gen/recording/television5.html

Figure captions

Figure 1: Simple target patterns as a function of offset ν_0 and maximum rf amplitude ν_1 are shown in A-D. For initial z magnetization, the desired orientation of the target magnetization vector M_t after the pulse is color coded: (white: $M_t = (1, 0, 0)$, black: M_t=(0,0,1)). For the corresponding optimized pulses shown in Fig. 2, simulated (A′-D′) and experimental (A″-D″) excitation profiles are presented, where the grey scale of the contour plots represents the actual x component of the final magnetization vector after the pulse (white: $M_x = 1$, black: $M_x = 0$).

Figure 2: Pulse amplitude and phase functions $s(t)$ and $\phi(t)$ of shaped pulses optimized to approach the target patterns shown in Fig. 1 A-D.

Figure 3: More complex target excitation pattern (A) and the corresponding simulated (B) and experimental (C) excitation profile of an optimized pulse.

Figure 4: Schematic representation of an experiment for the acquisition of the excitation profile as a function of offset ν_0 in a single shot. The investigated excitation pulse of duration T (grey rectangle) is applied in the presence of the gradient G_1. Immediately after the excitation pulse, x magnetization is brought back to the z axis by a time reversed broadband excitation pulse (BEBOP-tr) (18, 19, 20, 21), and during the delay δ any remaining transverse magnetization is dephased by applying a gradient G_2. Finally, in the presence of G_1, the stored z magnetization is rotated to the x axis by a BEBOP pulse and the FID is recorded.

Figure 5: Example of a specifically designed test pattern for the experimental calibration of rf amplitudes in a single shot, (A) target excitation pattern (white: $M_x = 1$, grey: $M_x = 0$, black: $M_x = -1$). In (B), the simulated excitation pattern of an optimized pulse is shown. At the rf amplitudes indicated by dashed horizontal lines (6.3 kHz, 7.4 kHz ,

8.7 kHz, 10.0 kHz, 11.2 kHz, 12.6 kHz, and 14.1 kHz, corresponding to attenuations of 4 dB, 2.6 dB, 1.2 dB, 0dB, -1 dB, -2 dB, and -3dB, respectively), the experimental single shot spectra shown in (C) were acquired.

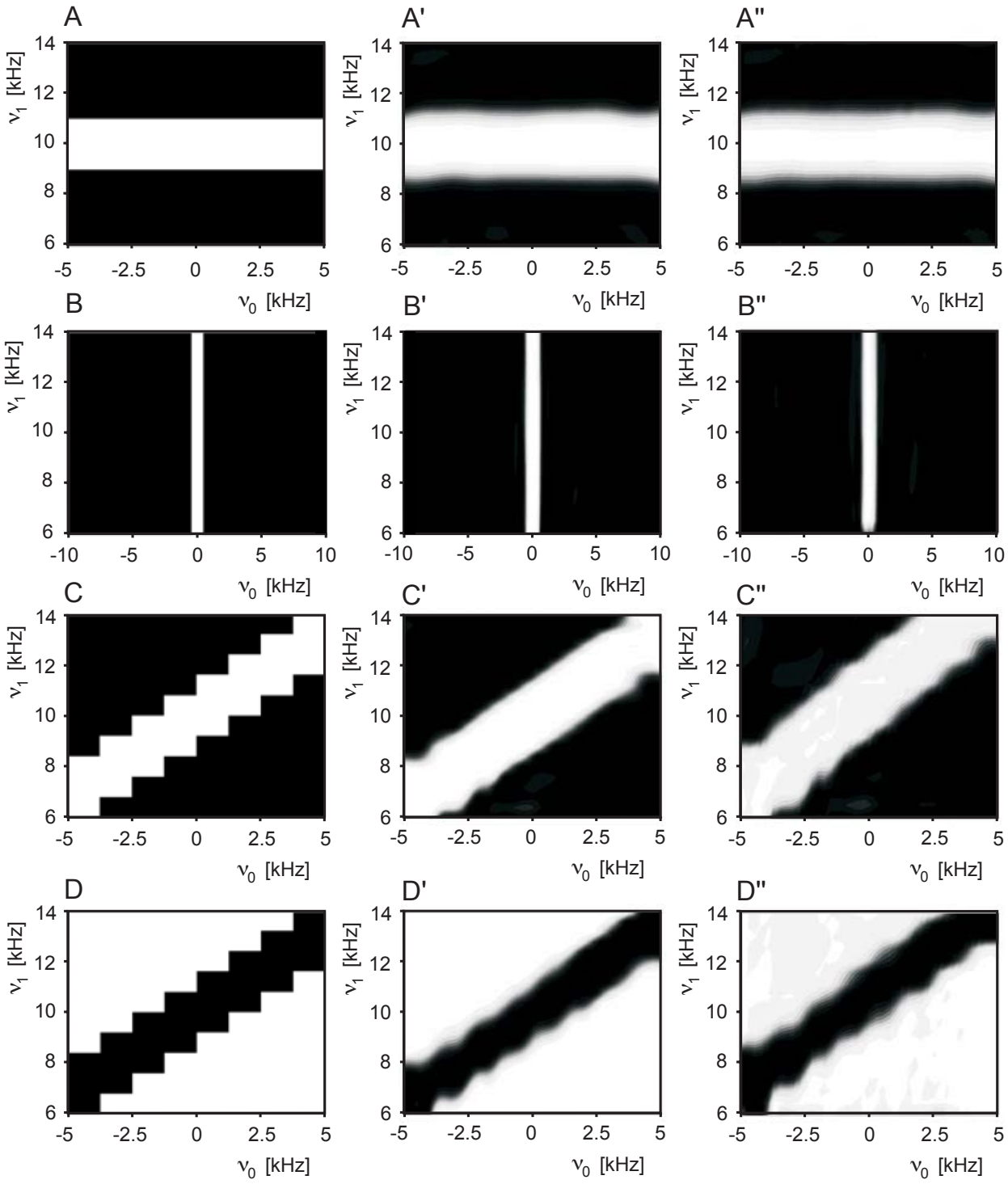

Figure 1

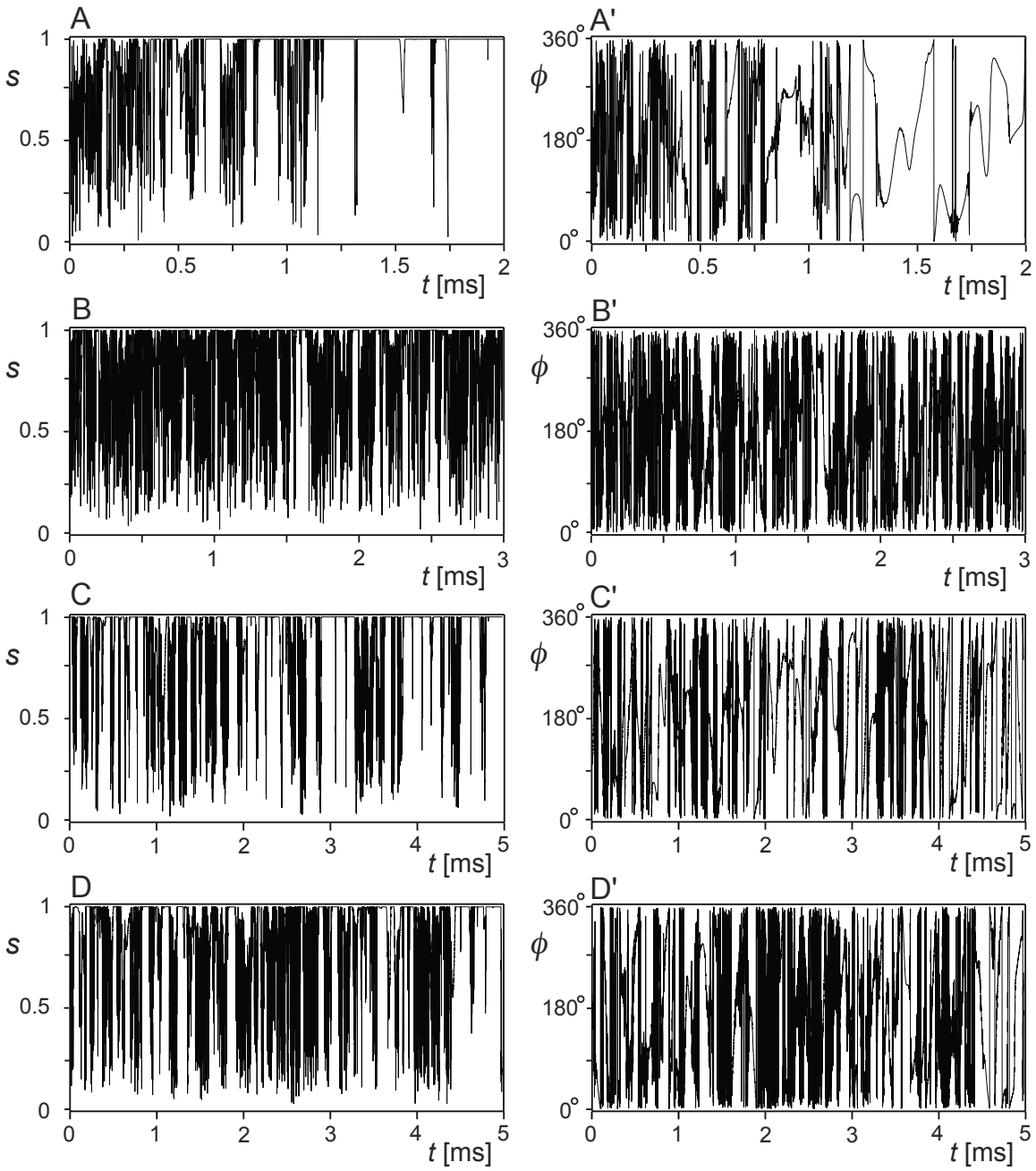

Figure 2

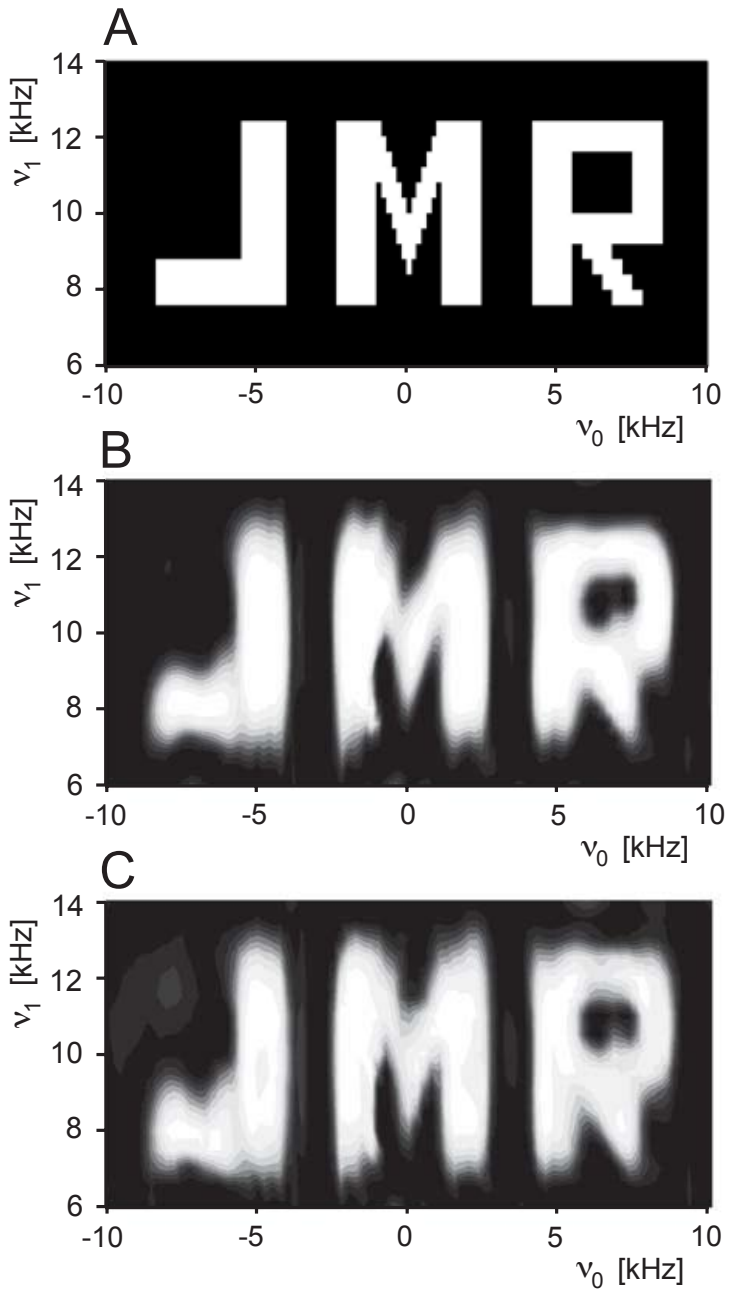

Figure 3

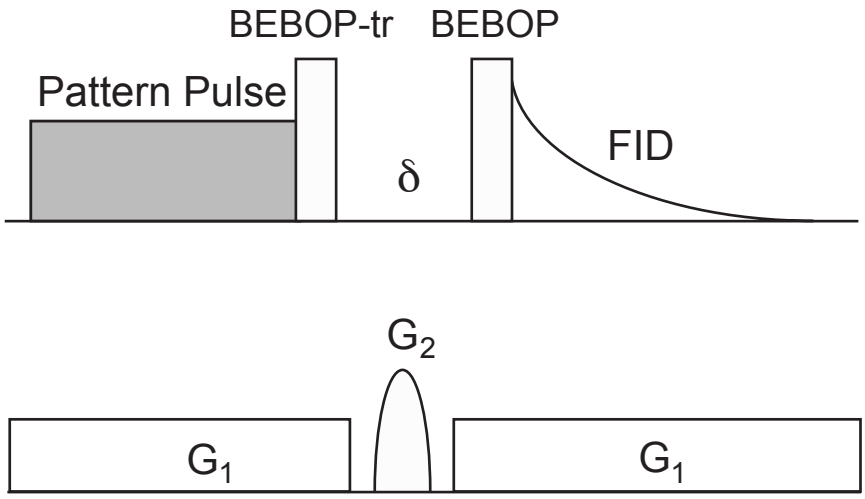

Figure 4

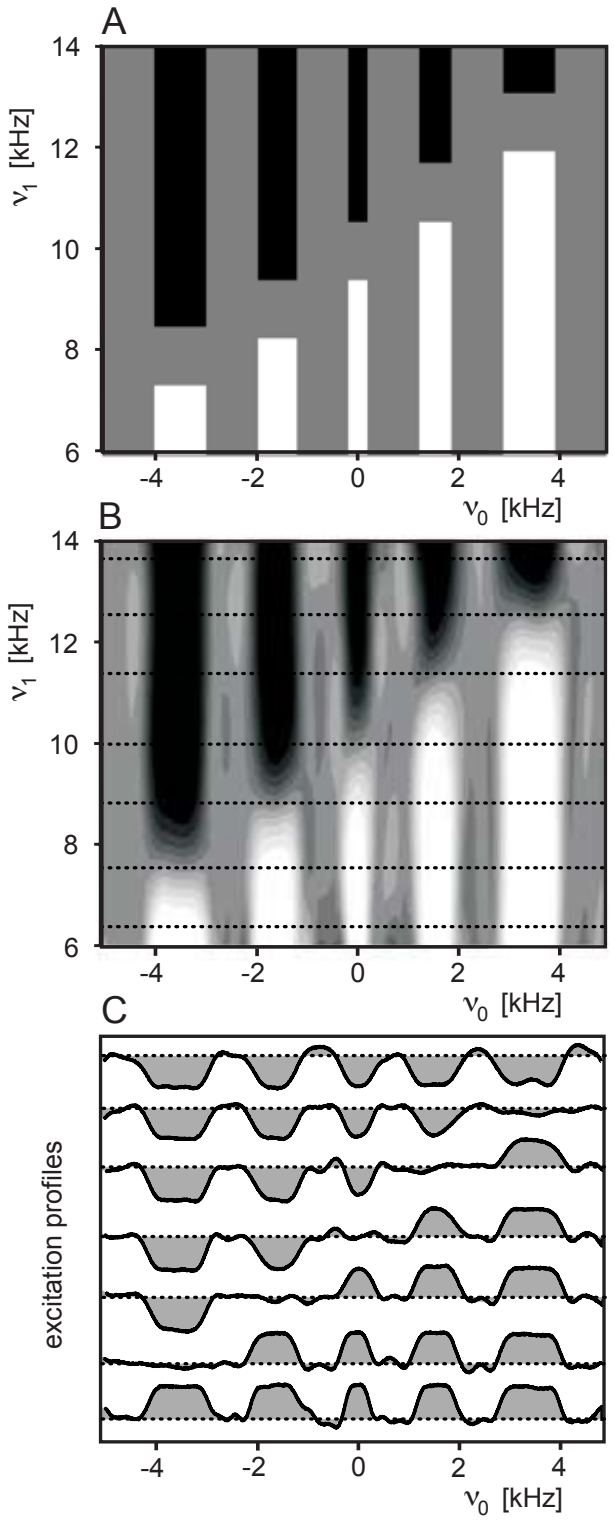

Figure 5